FEBS Letters 475 (2000) 218–224 FEBS 23807

Homogeneous longitudinal profiles and synchronous fluctuations of mitochondrial transmembrane potential

Giacomo Diaz*, Angela Maria Falchi, Fulvia Gremo, Raffaella Isola, Andrea Diana

Department of Cytomorphology, University of Cagliari, Cittadella Universitaria, 09042 Monserrato, Italy

Received 21 April 2000; received in revised form 23 May 2000

Edited by Vladimir Skulachev

Abstract This study reports for the first time (a) the longitudinal profile of the transmembrane potential (m$\Delta\psi$) of single mitochondria using a Nernstian fluorescent probe and (b) the distribution of m$\Delta\psi$ fluctuations of mitochondria undergoing permanent depolarization. Our findings show that (1) mitochondria in different energetic conditions coexist in the same cell, (2) m$\Delta\psi$ is rather homogeneous along the entire length of single mitochondria, (3) m$\Delta\psi$ is not influenced by the surrounding cytoplasmic environment and (4) m$\Delta\psi$ fluctuations occur simultaneously in groups of mitochondria connected in a network. Taken together, these findings provide further evidence for a functional relationship between mitochondrial arrangement and energetic condition.

Key words: Mitochondrion; Mitochondrial transmembrane potential; Potentiometric stain; Fluorescent probe; Image analysis

1. Introduction

Besides its key role in ATP synthesis, mitochondrial transmembrane potential (m$\Delta\psi$) is involved in other important processes such as calcium homeostasis [1,2], superoxide and free radical generation [3,4] and control of apoptosis [5,6]. m$\Delta\psi$ may be evaluated in intact cells using potential-sensitive fluorescent probes [7–9] and this method has made it possible to observe the coexistence of mitochondria in different energetic conditions in the same cell [10–15]. This point is of interest since mitochondrial depolarization may eventually result in the selective removal of no longer functional mitochondria from the cell [16,17] or in the death of the entire cell by apoptosis [18,19].

On the other hand, the m$\Delta\psi$ level often has an ambiguous meaning, as an m$\Delta\psi$ increase may be induced by a number of treatments such as the addition of oxidizable substrates, classically glutamate or succinate, inhibition of the electron transport chain with low rotenone [20], inhibition of ATP synthase by oligomycin [21] or hypoxia [17]. An m$\Delta\psi$ increase is also found in apoptosis, though restricted to a small fraction of mitochondria escaping early degeneration [15]. Even mtDNA-depleted and energetically inert mitochondria show a sustained m$\Delta\psi$ by a reverse ATP synthase activity on glycolytic ATP [22,23]. Inversely, an m$\Delta\psi$ decrease may result from substrate deprivation, augmented ATP demand, uncoupling factors and permeability transition pore opening [24].

A second problem of m$\Delta\psi$ evaluation concerns the sampling level. Up to now, m$\Delta\psi$ has been evaluated as a single overall estimate from all mitochondria present in a given cell [25,26] or as point estimates of individual mitochondria [11]. In no case has m$\Delta\psi$ been evaluated as multiple point estimates along the same mitochondrion, though this is indispensable information for comparing the m$\Delta\psi$ variations between and within different mitochondria by means of statistical tests [27]. This method, however, may be complicated by the degree of compactness and size of mitochondria [28,29]: it might be hard, for example, to assess the intramitochondrial m$\Delta\psi$ variability in the small, spherical mitochondria of liver cells or the intermitochondrial variability in the single, giant mitochondrial reticulum of adult skeletal muscle fibers [30]. On the other hand, the presence of different mitochondrial configurations in various tissues as well as in the same tissue in the course of differentiation suggests that a functional relationship must exist between mitochondrial structure and energetic condition. This hypothesis, which dates back to 1978 [30], has recently been confirmed by the finding that GTP binding proteins obtained from the outer mitochondrial membrane are able to induce mitochondrial hyperpolarization or mitochondrial fusion, depending on the G protein conformation [31]. At the same time, mitochondrial depolarization is frequently associated with mitochondrial fragmentation [32].

As regards the intramitochondrial m$\Delta\psi$ distribution, a theory formulated about 10 years ago by the group of Skulachev [33] assumes that m$\Delta\psi$ energy may be transduced along the inner mitochondrial membrane. A major experimental finding at the basis of the 'cable' theory was the evidence that irradiation or mechanical rupture through a narrow mitochondrial segment resulted in the depolarization of the entire mitochondrial filament [13,34]. In contrast to this phenomenon, the potentiometric probe JC-1 (5,5′,6,6′-tetrachloro-1,1′,3,3′-tetraethylbenzimidazolyl carbocyanine iodide) which is particularly appreciated for its chromatic response to low and high m$\Delta\psi$ levels [10,35] shows a discontinuous distribution which may be assumed to be indicative of the existence of sharp m$\Delta\psi$ differences along the same mitochondrion [13]. Neither point, however, appears to be conclusive: the first, because a diffuse depolarization consequent on local damage does not necessarily imply that m$\Delta\psi$ is homogeneous in the intact mitochondrion; the second, because the dashed pattern of JC-1 staining is probably a constitutive artifact due to the formation of J aggregates which, once initiated at sites with higher membrane density or larger matrix volume, have more chance to expand than new J aggregates to form in neighboring sites [36].

*Corresponding author. Fax: (39)-70-675 4003.
E-mail: gdiaz@unica.it

0014-5793/00/$20.00
PII: S0014-5793(00)01683-5

Considering all the above aspects of the problem, in this study we have investigated (a) the longitudinal mΔψ profiles of single mitochondria using the fluorescent probe TMRM (tetramethylrhodamine methyl ester) and (b) the mΔψ fluctuations of mitochondria exposed to prolonged probe excitation. Qualitative and quantitative data from both approaches converge toward the hypothesis that mΔψ is autonomously and homogeneously regulated in single mitochondria or in groups of mitochondria connected in a network.

2. Materials and methods

2.1. Cell treatments

Primary cultures of human fetal astrocytes and of adult fibroblasts and HEp2, Vero and KB cell lines were grown in Dulbecco's modified Eagle's medium (astrocytes, HEp2 and Vero) or RPMI (fibroblasts and KB). Cells were supravitally stained with 25 nM TMRM from a 25 μM dimethylsulfoxide stock solution, added to the culture medium 20 min before the observation and left in the medium during imaging sessions. The presence of the dye in the medium did not interfere with observations. Some cells were also stained with 100 nM nonyl-acridine orange (NAO) for 25 min. All probes were from Molecular Probes (Eugene, OR, USA).

2.2. Imaging

Observations were made with a Zeiss Axioskop microscope (Zeiss, Oberkochen, Germany) using a differential interference contrast Plan Achro 40×/0.75 NA water immersion objective. For fluorescence imaging, optical DIC components (polarizer, prism and condenser) were excluded. NAO and TMRM were observed with a standard set of filters for fluorescein (excitation 460–500, emission 510–560) and rhodamine (excitation 540–552, emission 590 LP), respectively. Eight bit, 1024×1024 grayscale images, embracing a field of 140 μm^2 (nominal resolution: 0.14 μm/pixel), were acquired by a class A Kodak Megaplus 1.4 slow scan camera (Eastman Kodak Co., San Diego, CA, USA) controlled by an IBAS 2000 image analyzer (Kontron Elektronik GmbH, Munich, Germany). Image analysis was done with Image-Pro Plus (Media Cybernetics, Silver Spring, MD, USA). Quantitative data were processed with Statistica (StatSoft, Inc., Tulsa, OK, USA) and NCSS (NCSS, Kaysville, UT, USA) statistical programs.

2.3. Sampling criteria

Longitudinal measurements were done on mitochondria which were (1) perfectly in focus, (2) regularly thick (not swollen, thinned, etc.), (3) regularly curved (not folded, wrinkled, etc.), (4) separated by more than 10 pixels from adjacent mitochondria. It was hard to distinguish continuity and simple contact of mitochondrial filaments in correspondence to bifurcations or crossing points. Thus, the sampled mitochondria do not necessarily represent separate or continuous structures. Indeed, separation (Fig. 1C: a, c, d) or continuity (Fig. 1C: pairs f and g, h and i, k and s) could be ascertained only in a few cases. On the other hand, inclusion in the analysis of some segments of the same mitochondrion should not invalidate the analysis; rather, it should reinforce the significance of the overall contrast between the average mΔψ of different mitochondrial segments.

The extent of lateral spread of the mitochondrial fluorescence was assessed with the potential-insensitive probe NAO to exclude or reduce the effect of the mitochondrial potential on the cytosolic concentration of the probe. NAO was used at a concentration able to produce a fluorescence intensity equivalent to that of TMRM. The lateral fluorescence was found to extend 7–10 pixels from the mitochondrial axis (Fig. 1B). The above sampling criteria were met only by mitochondria present in the peripheral cytoplasm of very large astrocytes and fibroblasts with a diameter exceeding 200 μm (Fig. 1C). In no case was sampling possible in cell lines due to the small size of cells and the extremely compact arrangement of mitochondria. In addition, the TMRM uptake was strongly conditioned in cell lines by a multidrug resistance-like behavior characterized by a large intercellular variability (manuscript submitted). For these reasons, the study was restricted to astrocytes and fibroblasts.

2.4. Acquisition of mitochondrial profiles

The image noise was evaluated from void fields of different fluorescence intensity using increasing TMRM concentrations in the pure medium. The standard deviation of fluorescence intensity was taken as overall noise estimate. A linear relationship was found between fluorescence intensity average and noise (standard deviation). Periodic and random noise components were also detected, but spatial and frequency filtering methods were not applied to whole images, due to the strong degradation of the thin mitochondrial traces. Noise was removed by a moving averaging of mitochondrial pixels within a circular mask of seven pixels of diameter moved along the mitochondrial axis (Fig. 1A). The size of the mask was optimized to fit the mitochondrial diameter. A conventional unit distance was assumed between consecutive step points, independently of the step orientation. Since the mean interpixel step distance along the eight directions is $(1+\sqrt{2})\times 4/8 = 1.2$ pixels, the length of mitochondrial traces is obtained as the number of steps×1.2×0.14 μm.

The circle-averaging method, tested on void fields, resulted in a 75% noise decrease. The residual noise, characterized by a mainly periodic component, was removed by an unweighted moving average of 21 elements. At this point the residual noise (standard deviation) was reduced to 0.5 units of gray values. This means that, assuming a normal distribution, the range of ±1 gray value (±2 S.D.) accounted for over 95% of the distribution. The length of the averaging segment (21 steps) was considerably shorter than the length of mitochondrial profiles (on average, 90 steps). This let a number of four to six mitochondrial segments be completely independent of each other, within each profile, without risk of variance underestimation.

2.5. mΔψ estimation

Assuming TMRM as an ideal Nernstian probe [11], mΔψ can be estimated by the equation $m\Delta\psi = -RT/ZF \times \ln (F_{mit}/F_{cyt})$, where R is the ideal gas constant, T is the absolute temperature, Z is the ionic charge, F is the Faraday constant, F_{mit} is the mitochondrial fluorescence intensity and F_{cyt} is the extramitochondrial fluorescence intensity. The latter was sampled in peripheral regions of the cell, free of mitochondria and endoplasmic reticulum. At 30°C, using common logarithms and expressing data in mV, the expression becomes $m\Delta\psi = -60 \times \log (F_{mit}/F_{cyt})$.

Compensation for the mΔψ underestimation due to the mitochondrial fluorescence dilution in the microscope focus depth, proposed by Loew and co-workers [9,11], was omitted. This compensation consists in a correction factor applied to the F_{mit}/F_{cyt} ratio, based on the microscope point spread function. The logarithmic function makes the correction factor equivalent to an additive term which shifts the datum along the mΔψ scale. Indeed, values calculated by the Nernst equation were already in the physiological range, so we considered the possibility that F_{mit} values could have been inflated or in some way altered by (a) spurious fluorescence spreading from adjacent or out-of-focus mitochondria, (b) non-potentiometric probe binding or (c) changes in the mitochondrial thickness. These hypotheses appeared in contrast to (1) the short range of lateral fluorescence spread, as shown in Fig. 1B, (2) the checked absence of out-of-focus mitochondria, due also to the high degree of cell spreading, (3) the observation of consistent differences even between adjacent mitochondria (Fig. 1C, inset; Fig. 3, encircled data), (4) the complete destaining following treatment with 10 μM CCCP which excluded the presence of appreciable potential-insensitive binding (data not shown) and (5) the homogeneous staining obtained with the non-potentiometric probe NAO. Finally, since results of statistical tests, variability parameters and value changes, which are the main object of this study, are invariant to linear operations, we preferred to not correct original data, leaving open the possibility of a consistent adjustment of their location on the mV scale.

The same considerations were made in relation to the quasi-linear deviation of data from the Nernst equation due to a low but significant potential-sensitive binding of TMRM [26]. However, all data were processed in parallel by parametric (ANOVA) and non-parametric (Kruskal–Wallis) tests to exclude the influence to non-linear changes.

2.6. Analysis of mΔψ fluctuations

In the center of the cell, where sampling of single mitochondrial traces was prevented by the compact arrangement of mitochondria, the analysis was directed to evaluate the fluorescence fluctuations

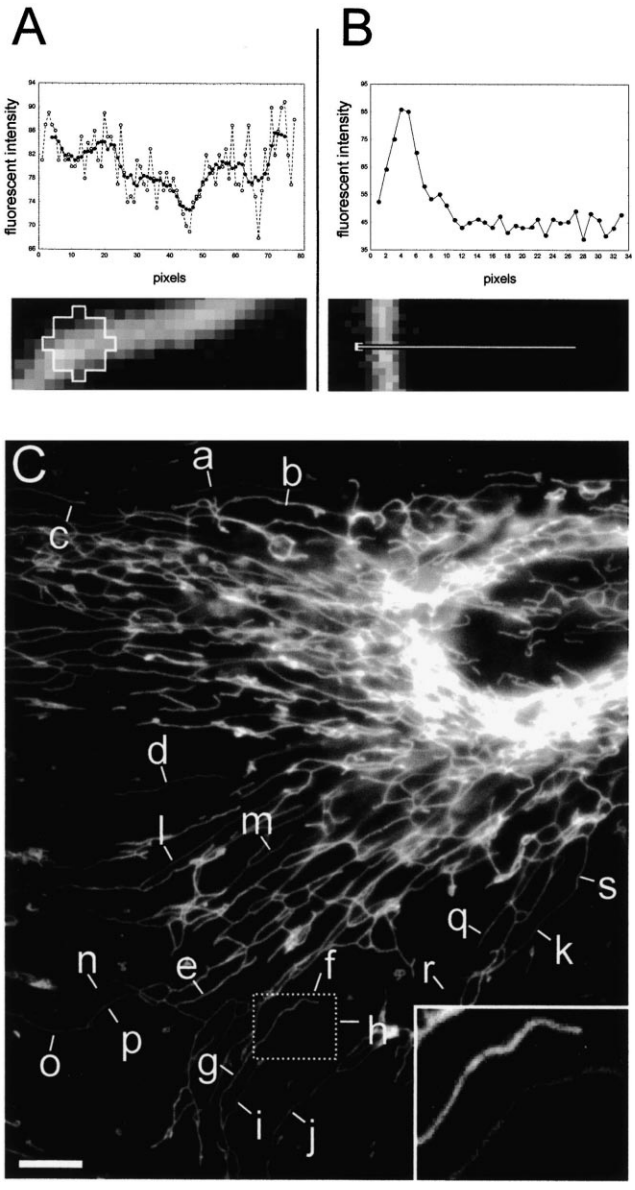

Fig. 1. A: Circular mask of seven pixels of diameter used to scan TMRM-stained mitochondria. Since the pixel size is 0.14 μm, the mask measures about 1 μm in diameter. For each consecutive mask position, fluorescence intensities of the matched pixels are averaged. The sequence of averaged values forms the final mitochondrial profile. The plot shows the effect of mask averaging (thick trace) versus single pixel values (dotted trace). B: The lateral spread of mitochondrial fluorescence was evaluated by a line profile across the mitochondrial axis. The curve shows that fluorescence spread is virtually null at the distance of about eight pixels from the peak (pixels 4–5 of the plot) of the mitochondrial axis. C: Astrocyte stained with TMRM. Letters (a–s) label mitochondria selected for the analysis. Fluorescence profiles and summary statistics are shown in Figs. 2 and 3. The inset is an enlargement of the small framed area showing two adjacent mitochondria (f and h) with consistently different levels of fluorescence intensity. Bar = 10 μm.

occurring in specific areas of the mitochondrial network after prolonged exposure to the excitation light and preceding the permanent depolarization. Serial images were initially acquired at different time intervals (from 500 ms to 30 s). The phenomenon appeared to be adequately sampled by a time lapse of 10 s. The relative $m\Delta\psi$ change occurring in a mitochondrial area at a given time x ($m\Delta\Delta\psi_x$) was evaluated as

$$m\Delta\Delta\psi = [-60\times\log(F_{mit_x}/F_{cyt_x})]-[-60\times\log(F_{mit_{x-1}}/F_{cyt_{x-1}})]$$

where F_{mit_x}/F_{cyt_x} and $F_{mit_{x-1}}/F_{cyt_{x-1}}$ are the fluorescence ratios of two consecutive images taken at times $x-1$ and x, respectively. Assuming that cytosolic fluorescence does not change between times $x-1$ and x, the equation may be reduced to $m\Delta\Delta\psi_x = -60\times\log(F_{mit_x}/F_{mit_{x-1}})$.

3. Results

Plots of mitochondrial $m\Delta\psi$ profiles (Fig. 2) seem to indicate a more homogeneous distribution of data within the same mitochondrion than between different mitochondria. Distribution plots (Fig. 3) and statistical tests confirmed this impression. The non-parametric Kruskal–Wallis test (more suitable than the one-way ANOVA, owing to the strong deviations from normality) provided, in all six cases, the lowest computable probability ($\alpha < 0.000001$) for the hypothesis of equal $m\Delta\psi$ medians. This is equivalent to saying that the $m\Delta\psi$ variability at the intermitochondrial level is significantly larger than that found at the intramitochondrial level. To rule out the suspicion of bias due to the application of moving averaging or to a less conservative behavior of the non-parametric method, the Kruskal–Wallis test and ANOVA were applied to mitochondrial profiles with and without data averaging. All 24 combinations of test (parametric/non-parametric) and pro-

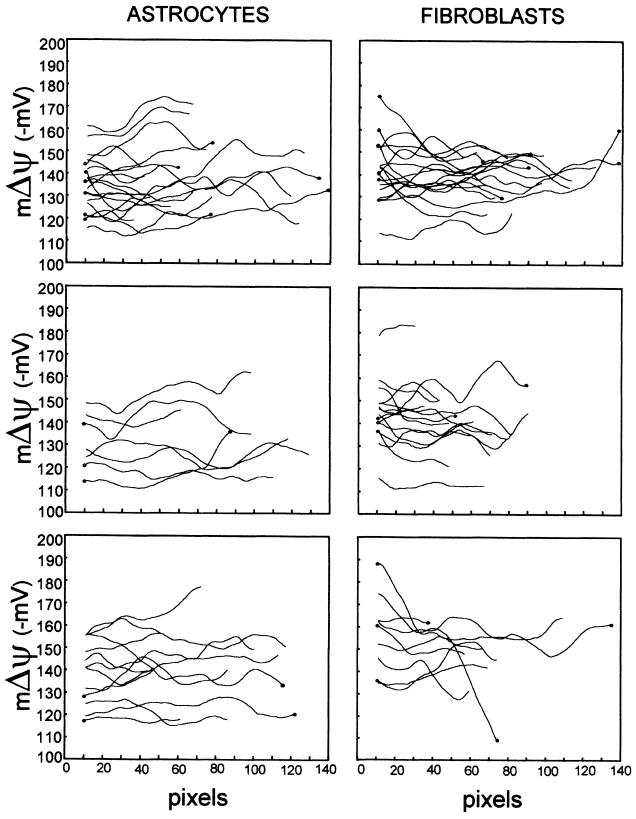

Fig. 2. Longitudinal $m\Delta\psi$ profiles of 80 mitochondria sampled from three human astrocytes and three human fibroblasts. Profile extremities corresponding to natural ends are terminated by small dots. In all other cases, profile extremities correspond to truncations of mitochondrial traces due to sampling conditions. A large intermitochondrial variability is evident. At the intramitochondrial level, major deviations tend to be localized in correspondence to mitochondrial ends.

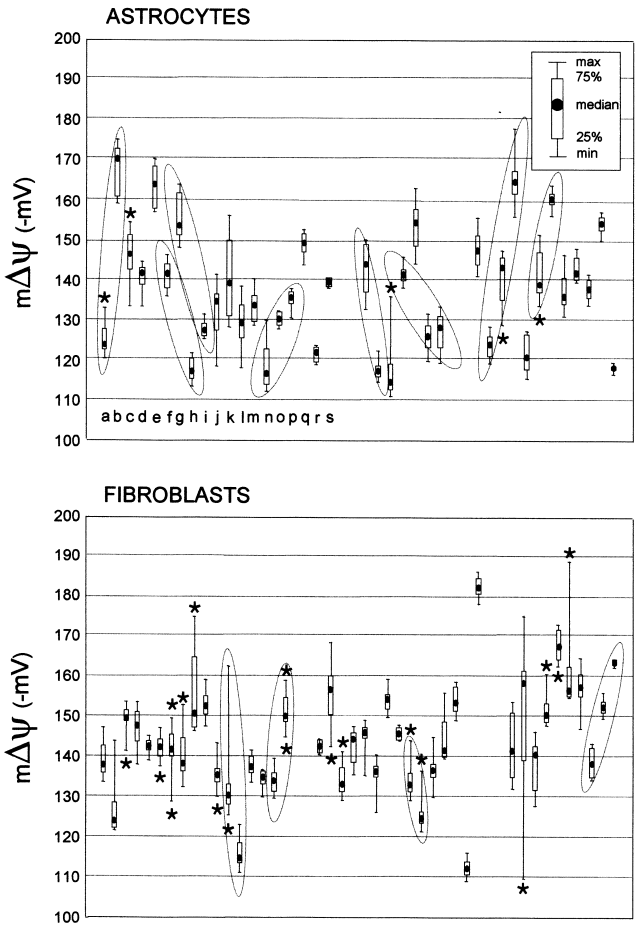

Fig. 3. Summary statistics of mΔψ profiles. The first 19 plots (upper graph, labels a–s) refer to mitochondria shown in Fig. 1C. Asterisks near to min–max limits indicate that the corresponding mΔψ minimum or maximum was localized in a mitochondrial end. Elliptical outlines include plots of mitochondria found in side-by-side, adjacent positions.

cessing methods (averaging/no averaging) applied to the six data sets gave identical results (in all cases, $\alpha < 0.000001$).

The average mΔψ of mitochondrial profiles was -137 ± 14 mV (mean ± S.D.) in astrocytes and -143 ± 13 mV in fibroblasts. These values are somewhat lower than those found in neuroblastoma neurites (average: 150 ± 11 mV) by Loew and co-workers using the same probe [11]. However, the difference may be ascribed to a mΔψ underestimation due to the use of wide-field images (see Section 2.5). Standard deviations, which are not sensitive to scale shifts, are in better agreement. The larger mΔψ variability found in astrocytes and fibroblasts versus neuroblastoma cells may be ascribed to the broader heterogeneity of mitochondrial conditions correlated with the rapid ageing of primary cultures versus cell lines.

At the intramitochondrial level, standard deviations were 3.8 mV in astrocytes and 4.5 mV in fibroblasts. Comparative data are not available in the literature. A major component of this variability was localized in the mitochondrial ends. The frequency of mitochondrial ends displaying mΔψ maxima was 16% in astrocytes and 39% in fibroblasts. The frequency of mitochondrial ends displaying mΔψ minima was 11% in astrocytes and 39% in fibroblasts. In total, 27% of mitochondrial ends of astrocytes and 78% of mitochondrial ends of fibroblasts showed extreme values of the intramitochondrial distributions.

mΔψ was not correlated with the mitochondrial location within the cell, as conspicuous mΔψ differences were found even between closely adjacent mitochondria (Fig. 1C, inset and Fig. 3).

An interesting aspect of mΔψ profiles was the absence of plateau levels. This ensured that measurements were in the range of TMRM sensitivity and, at the same time, excluded the occurrence of physiological thresholds at least in the range of the observed values.

Mitochondrial fluorescence was rather stable during the first minute of continuous exposure to the excitation light. After this period, a brusque destaining and a rapid redistribution of TMRM in the cell was generally observed. The time of mitochondrial destaining depended on the absolute, dose-related TMRM concentration in mitochondria more than on the mΔψ-related mitochondrial/cytosolic ratio, in agreement

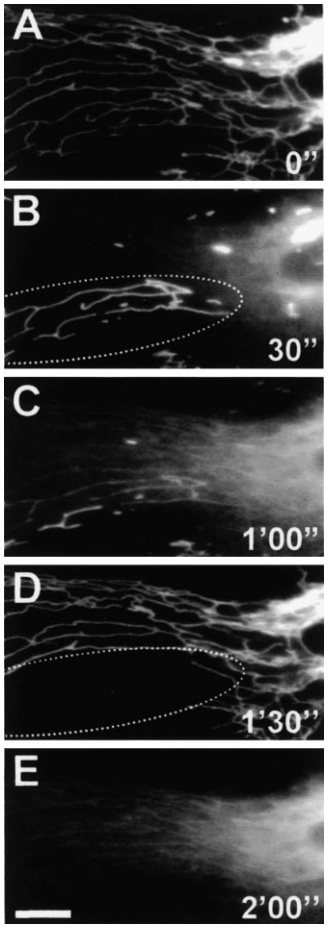

Fig. 4. Large mΔψ fluctuations in a TMRM-stained astrocyte exposed to continuous excitation. The five images were taken at time intervals of 30 s. A: The mitochondrial network is entirely stained. The intense fluorescence on the right corresponds to the perinuclear region. B: A large portion of the mitochondrial network is depolarized. A massive TMRM efflux from the perinuclear network is evident. The remaining portion of the network is still polarized (encircled). C: The situation is inverting. D: Polarization is resumed by the larger portion of mitochondrial network, whereas it is lost by the smaller one (encircled). E: All mitochondria are depolarized. Bar = 10 μm.

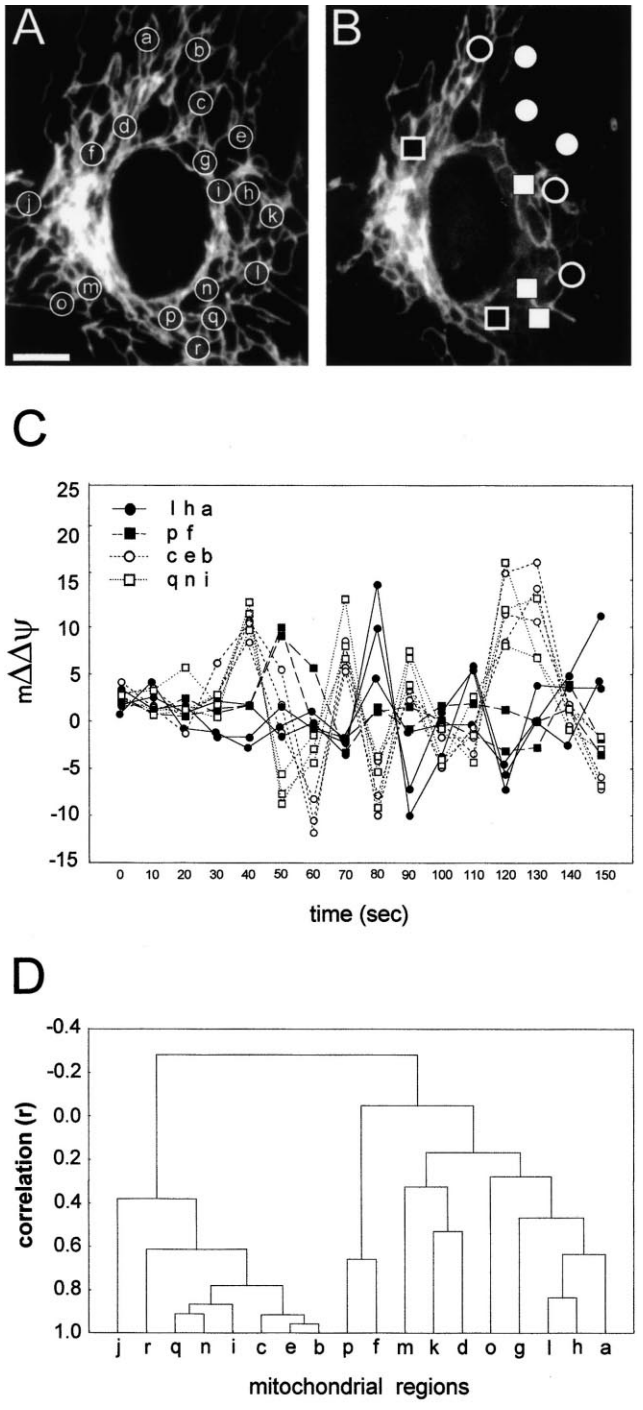

Fig. 5. Analysis of mΔψ fluctuations in a TMRM-stained astrocyte exposed to continuous illumination for 150 s. Images were taken every 10 s. A: Initial image. The perinuclear cytoplasm is subdivided into 18 small areas (a–r, referenced also in C and D) excluding regions with too high or low mitochondrial densities. Bar = 10 μm. B: Last image. Four groups of areas with correlated mΔψ fluctuations are mapped: l-h-a [●]; p-f [■]; c-e-b [○]; and q-n-i [□]. Note the total depolarization of the c-e-b group and the considerable distance between areas of the l-h-a group. C: Plot of mΔψ changes (mΔΔψ) between consecutive images. For clarity, only data of the 11 most correlated areas are shown. A near alternate phasing of mΔψ fluctuations is evident. D: Linkage map of the 18 mitochondrial areas obtained by cluster analysis, based on pairwise correlations between mΔΔψ sequences and the unweighted pair group method. The four clusters of mitochondrial areas with the most correlated mΔψ fluctuations are easily identified: c-e-b, q-n-i, l-h-a and p-f (in order of decreasing correlation). These clusters are mapped in B.

with analogous observations on isolated mitochondria [37] and consistent with the hypothesis of generation of reactive oxygen species by the probe excitation [38] and the consequent permeabilization of the mitochondrial membrane [39]. However, in many cases, staining was cyclically resumed and lost again by mitochondria before their permanent depolarization. These fluctuations could be optimally monitored at time intervals of 10 s, with cells under constant illumination. No fluorescence waves were detected along the length of mitochondria undergoing fluctuations. In some cases, mΔψ fluctuations involved large portions of the mitochondrial network, clearly evident to the observer during acquisition of images (Fig. 4). In other cases, fluctuations were less intense and restricted to small mitochondrial areas, so that they could be detected only by comparative analysis of images (Fig. 5A). For this purpose, the mitochondrial mass surrounding the nucleus was subdivided into small areas and each area separately evaluated. Surprisingly, plots of fluorescence intensities of consecutive images revealed synchronous fluctuations in distinct mitochondrial areas (Fig. 5C). These were objectively recognized by cluster analysis (Fig. 5D). Mitochondrial areas with synchronous fluctuations were sometimes found at a remarkable distance from each other, suggesting the existence of distinct mitochondrial networks within the whole mitochondrial tangle. mΔψ fluctuations ended with the final depolarization of mitochondria, but also in this case, mitochondria with synchronous fluctuations reached depolarization at different times. At this point, the contrast between the depolarized and still polarized areas made it possible to detect the structural continuity between mitochondrial areas which had exhibited synchronous fluctuations (Fig. 5B) and to confirm the linkage map obtained by cluster analysis.

4. Discussion

This investigation reports for the first time the longitudinal mΔψ profiles of single mitochondria. Unfortunately, the need to observe cells with particular morphological characteristics, such as an extremely spread cytoplasm and long mitochondria radiating from the center toward the cell periphery, excluded from this investigation all cell lines which are preferentially adopted for studies on the energetic metabolism using isolated mitochondria, and this could in theory limit the scope of our conclusions. On the other hand, the good agreement between data of such widely differing cell types as astrocytes and fibroblasts should allow some generalization of results.

The analysis of mΔψ profiles shows that mΔψ is homogeneously distributed within mitochondria. The lack of correlation between mitochondrial potential and location and the frequent contrast between the entire length of adjacent mitochondria suggest that mitochondria are autonomous organelles, not influenced by the surrounding cytoplasm.

Quantitative data are substantiated by the rather long extension of the mitochondrial traces examined, in many cases exceeding the size of 15 μm. The relatively small intramitochondrial mΔψ variability may be ascribed to irregularities of the mitochondrial thickness, not morphologically recognizable at the light microscope resolution. Indeed, major intramitochondrial differences were found in the mitochondrial ends, where dilations or contractions of the mitochondrial diameter are more frequently found.

An explanation for the intramitochondrial mΔψ homogene-

ity may be found in the large-range lateral diffusion of integral proteins of the inner mitochondrial membrane, postulated by the random collision model of mitochondrial electron transport [40–42]. The linear displacement of redox components, estimated from their diffusion coefficients, is of the order of some μm/s [43,44]. A second mechanism which may favor the propagation of the prevailing (low or high) $m\Delta\psi$ condition is the voltage-dependent behavior of mitochondrial permeability transition pores which tend to close at high, physiological $m\Delta\psi$ and to open after depolarization [45]. Our data are also compatible with the theory formulated by Skulachev [33] which assimilates mitochondrial membranes to cables capable of transmitting energy, though our data are not unequivocally associated with this theory.

Particular emphasis has been ascribed in the past to the $m\Delta\psi$ loss of entire mitochondria induced by laser irradiation across a narrow mitochondrial segment [13,33,34]. Sometimes, the irradiation-induced $m\Delta\psi$ loss was followed by a recovery both in mitochondria of intact cells [11] and in isolated mitochondria [37]. However, the two events, the $m\Delta\psi$ loss and its subsequent recovery, have different implications. In fact, the first loss may be the simple consequence of a specific permeability transition pore opening or of a less specific mechanism of permeabilization of the inner mitochondrial membrane due to oxidative damage [3,16,46]. In this case the mitochondrion is completely passive. On the other hand, the $m\Delta\psi$ recovery requires an active intervention of the mitochondrion for the re-establishment of a consistent $m\Delta\psi$ over its entire length. The fact that an $m\Delta\psi$ recovery in studies with intact cells has been observed only in a few circumstances [11] supports this distinction. The high frequency of $m\Delta\psi$ recoveries observed in our experiments may depend on the moderate irradiation intensity of the 50 W mercury lamp used in wide-field microscopy, certainly less destructive than that produced by the laser beam of a confocal microscope. Indeed, we often observed series of fluctuations in different mitochondria. The structural link between mitochondria with synchronous fluctuations, evident at the time of the final depolarization, suggests the existence of distinct mitochondrial subnetworks within the intricate mass of mitochondria surrounding the nucleus. Although it cannot be excluded that these subnetworks may result from the cleavage of a continuous mitochondrial structure due to the same phototoxic injury, the variety of situations observed under constant experimental conditions seems more compatible with the hypothesis of a pre-existent separation of mitochondria.

The ability to divide or to fuse into a variety of configurations is a well known characteristic of mitochondria, documented in over a century of morphological investigations [28,29,47]. However, despite the very large number of studies, the mechanism and meaning of mitochondrial plasticity is still unknown. Recent experimental data have shown that mitochondrial fusion can be modulated by GTP binding proteins obtained from the mitochondrial membrane and that mitochondrial fusion is correlated with a $m\Delta\psi$ change [31]. The hypothesis of a functional relationship between the energized condition and morphological configuration of mitochondria is well consistent with our findings.

References

[1] Budd, S.L. and Nicholls, D.G. (1996) J. Neurochem. 66, 403–411.
[2] Babcock, D.F., Herrington, J., Goodwin, P.C., Park, Y.B. and Hille, B. (1997) J. Cell Biol. 136, 833–844.
[3] Budd, S.L., Castilho, R.F. and Nicholls, D.G. (1997) FEBS Lett. 415, 21–24.
[4] Korshunov, S.S., Skulachev, V.P. and Starkov, A.A. (1997) FEBS Lett. 416, 15–18.
[5] Zamzami, N., Marchetti, P., Castedo, M., Zanin, C., Vayssiere, J.L., Petit, P.X. and Kroemer, G. (1995) J. Exp. Med. 181, 1661–1672.
[6] Heiskanen, K.M., Bhat, M.B., Wang, H.W., Ma, J. and Nieminen, A.L. (1999) J. Biol. Chem. 274, 5654–5658.
[7] Bereither-Hahn, J. (1990) Int. Rev. Cytol. 122, 1–63.
[8] Reers, M., Smith, W.S. and Chen, L.B. (1991) Biochemistry 30, 4480–4486.
[9] Fink, C., Morgan, F. and Loew, L.M. (1998) Biophys. J. 75, 1648–1658.
[10] Smiley, S.T., Reers, M., Mottola-Hartshorn, C., Lin, M., Chen, A., Smith, T., Steele, G.D. and Chen, L.B. (1991) Proc. Natl. Acad. Sci. USA 88, 3671–3675.
[11] Loew, L., Tuft, R.A., Carrington, W. and Fay, F.S. (1993) Biophys. J. 65, 2396–2407.
[12] Kirischuck, S., Neuhaus, J., Verkhratsky, A. and Kettenmann, H. (1995) NeuroReport 6, 737–741.
[13] Bereither-Hahn, J. and Vöth, M. (1998) Exp. Biol. Online 3, 12–27.
[14] Dedov, V.N. and Roufogalis, B.D. (1999) FEBS Lett. 456, 171–174.
[15] Diaz, G., Setzu, M.D., Zucca, A., Isola, R., Diana, A., Murru, R., Sogos, V. and Gremo, F. (1999) J. Cell Sci. 112, 1077–1084.
[16] Skulachev, V.P. (1996) FEBS Lett. 397, 7–10.
[17] Broekemeier, K.M., Klocek, C.K. and Pfeiffer, D.R. (1998) Biochemistry 37, 13059–13065.
[18] Zamzami, N., Susin, S.A., Marchetti, P., Hirsch, T., Gomez-Monterrey, I., Castedo, M. and Kroemer, G. (1996) J. Exp. Med. 183, 1533–1544.
[19] Susin, S.A., Zamzami, N. and Kroemer, G. (1998) Biochim. Biophys. Acta 1366, 151–165.
[20] Barrientos, A. and Moraes, C.T. (1999) J. Biol. Chem. 274, 16188–16197.
[21] Ichas, F., Jouaville, L.S. and Mazat, J.-P. (1997) Cell 89, 1145–1153.
[22] Skowronek, P., Haferkamp, O. and Rödel, G. (1992) Biochem. Biophys. Res. Commun. 187, 991–998.
[23] Buchet, K. and Godinot, C. (1998) J. Biol. Chem. 273, 22983–22989.
[24] Gunter, T.E. and Pfeiffer, D.R. (1990) Am. J. Physiol. 258, C755–C786.
[25] Ubl, J.J., Chatton, J., Chen, S. and Stucki, J.W. (1996) Biochim. Biophys. Acta 1276, 124–132.
[26] Scaduto Jr., R.C. and Grotyohann, L.W. (1999) Biophys. J. 76, 469–477.
[27] Snedecor, G.W. and Cochran, W.G. (1980) Statistical Methods, 7th edn., Iowa State University Press, Ames, IA.
[28] Tandler, B. and Hoppel, C.L. (1972) Mitochondria, Academic Press, New York.
[29] Bereither-Hahn, J. and Vöth, M. (1994) Microsc. Res. Tech. 27, 198–219.
[30] Bakeeva, L.E., Chentsov, Y.S. and Sculachev, V.P. (1978) Biochim. Biophys. Acta 501, 349–369.
[31] Cortese, J.D. (1999) Am. J. Physiol. 276, C611–C620.
[32] Vorobjev, I.A. and Zorov, D.B. (1983) FEBS Lett. 163, 311–314.
[33] Skulachev, V.P. (1990) J. Membr. Biol. 114, 97–112.
[34] Amchenkova, A.A., Bakeeva, L.E., Chentsov, Y.S., Skulachev, V.P. and Zorov, D.B. (1988) J. Cell Biol. 107, 481–485.
[35] Chen, L.B. and Smiley, S.T. (1993) in: Fluorescent and Luminescent Probes for Biological Activity (Mason, W.T., Ed.), pp. l24–132, Academic Press, London.
[36] Kawasaki, M. and Inokuma, H. (1999) J. Phys. Chem. B 103, 1233–1241.
[37] Hüser, J., Rechenmacher, C.E. and Blatter, L.A. (1998) Biophys. J. 74, 2129–2137.

[38] Tsien, R.Y. and Waggoner, A. (1995) in: Handbook of Biological Confocal Microscopy (Pawley, J.B., Ed.), pp. 267–280, Plenum Press, New York.
[39] Valle, V.G.R., Fagian, M.M., Parentoni, L.S., Meinicke, A.R. and Vercesi, A.E. (1993) Arch. Biochem. Biophys. 307, 1–7.
[40] Hackenbrock, C.R. (1981) Trends Biochem. Sci. 6, 151–154.
[41] Hackenbrock, C.R., Chazotte, B. and Gupte, S.S. (1986) J. Bioenerg. Biomembr. 18, 331–368.
[42] Chazotte, B. and Hackenbrock, C.R. (1989) J. Biol. Chem. 264, 4978–4985.
[43] Sowers, A.E. and Hackenbrock, C.R. (1981) Proc. Natl. Acad. Sci. USA 78, 6246–6250.
[44] Gupte, S.S., Chazotte, B., Leesnitzer, M.A. and Hackenbrock, C.R. (1991) Biochim. Biophys. Acta 1069, 131–138.
[45] Bernardi, P. (1992) J. Biol. Chem. 267, 8834–8839.
[46] Vercesi, A.E., Kowaltowski, A.J., Grijalba, M.T., Meinicke, A.R. and Castilho, R.F. (1997) Biosci. Rep. 17, 43–52.
[47] Altmann, R. (1890) Die Elementarorganismen und ihre Beziehungen zu den Zellen, Veit, Leipzig.